Synthesis, Structure and Magnetic Properties of a New Iron Arsenate, $[C_{10}N_4H_{28}][\{FeF(OH)(HAsO_4)\}_4]$, with a Layer Structure

Sandip Chakrabarti,[a] Swapan K. Pati,[b] Mark A. Green,[c] and Srinivasan Natarajan*[a]

Keywords: Iron / Arsenic / Solvothermal synthesis / N ligands

The reaction of $FeCl_3 \cdot 6H_2O$, H_3AsO_4, HF and 1,4-bis(3-aminopropyl)piperazine under solvothermal conditions gives rise to a new iron arsenate, $[C_{10}N_4H_{28}][\{FeF(OH)(HAsO_4)\}_4]$ (**I**) with a layered structure. The cell parameters are monoclinic, space group = $P2_1/n$ (no.14), M = 1143.08, a = 9.6320(3), b = 8.3598(3), c = 10.7794(1) Å, β = 115.036(1)°, V = 786.42(4) Å^3, Z = 4, R_1 = 0.0492, wR_2 = 0.1227 [1114 observed reflections with $I > 2\sigma(I)$]. The connectivity between $FeO_3F_2(OH)$ octahedra and $HAsO_4$ tetrahedra forms a secondary building unit (SBU) of the type SBU-4. The SBU-4 units are linked together to form a layer structure with apertures formed by 8-T atoms (T = Fe, As). The amine molecules are disordered and occupy the inter-lamellar region. To the best of our knowledge, **I** is the first example of an iron arsenate structure formed from only one type of secondary building unit, SBU-4. A dimer model has been used to describe the magnetic behavior.

Introduction

The synthesis, structure and properties of metal phosphates prepared in the presence of organic amines has been intensely researched during the last two decades.[1] Of these, the transition metal phosphates are interesting due to the variations in the oxidation state and coordination preferences of the transition element. Thus, a large number of iron phosphates with novel structures have been prepared and characterized.[2,3] Most of these iron phosphates have been prepared by employing hydrothermal methods. In some cases HF was used as the mineralizer, which also becomes part of the structure by linking the metal centers.[2−4] It is interesting to note that the use of HF produced a number of novel phosphate frameworks that do not generally form in the fluoride-free medium.

Though arsenic belongs to the same group as phosphorous, little work has been carried out on arsenate-based framework structures. It is likely that the larger size of the As^{5+} cation (0.335 Å) compared to the P^{5+} cation (0.17 Å)[5] would lead to the formation of completely different structures. In addition, a comparison of the pK_a values of H_3PO_4 and H_3AsO_4 also gives an idea about the relative ease of removal of protons. Thus for H_3PO_4, pK_{a1}, pK_{a2} and pK_{a3} are 2.12, 7.21 and 12.32, respectively, while for H_3AsO_4, pK_{a1}, pK_{a2} and pK_{a3} are 2.3, 6.9 and 11.5, respectively. This probably indicates that arsonic acid is somewhat weaker than phosphoric acid. The research in arsenate-based framework compounds are beginning to emerge, but is limited possibly due to the toxicity associated with arsenic and its relative inability to form extended networks. The intense investigations by many researchers during the last decade or so have given rise to new arsenates of different compositions and structures. Thus, arsenates of aluminum,[6,7] gallium,[8−10] molybdenum,[11,12] vanadium,[13−18] iron[19−24] and zinc[25−27] have been prepared and their structures reported in the literature. In order to expand the family of known arsenate framework structures, we have been investigating the formation of iron arsenates in the presence of structure-directing organic amine molecules. In this paper, we report the hydrothermal synthesis, crystal structure and spectroscopic and magnetic properties of a new iron(III) arsenate prepared in the presence of 1,4-bis(3-aminopropyl)piperazine (AP-PIP) cations, $[C_{10}N_4H_{28}][\{FeF(OH)(HAsO_4)\}_4]$ (**I**). This compound possesses a layer structure formed entirely by the linking between only one type of secondary building units (SBU-4),[28,29] which to the best of our knowledge is the first example of an iron arsenate formed with organic cations.

[a] Framework Solids Laboratory, Chemistry and Physics of Materials Unit, Jawaharlal Nehru Centre for Advanced Scientific Research,
Jakkur P. O., Bangalore 560 064, India
Fax: (internat.) +91-80/846-2766, 856-6581
E-mail: raj@jncasr.ac.in
[b] Theoretical Sciences Unit, Jawaharlal Nehru Centre for Advanced Scientific Research,
Jakkur P. O., Bangalore 560 064, India
[c] Davy-Faraday Research Laboratory, The Royal Institution of Great Britain, 21
Albemarle Street, London W1S 4BS, UK

Results and Discussion

The structure consists of macroanionic layers of $[\{FeF(OH)(HAsO_4)\}_4]^{4-}$ formed by the linking of FeO_4-

  DOI: 10.1002/ejic.200300237

F(OH) octahedra and $AsO_3(OH)$ tetrahedra. The AP-PIP cations are located in the inter-lamellar region. The asymmetric unit of the layer is shown in Figure 1. There is only one crystallographically distinct Fe and As atom in the asymmetric unit. The Fe atom is octahedrally coordinated by four O and two F atoms with Fe−O/F bond lengths in the range 1.884(6)−2.049(5) Å (av. 1.9842 Å). The octahedral O/F−Fe−O/F bond angles are in the range 77.6(2)−176.3(3)° (av. 106.3°). The iron atom is linked to the arsenic atom by three Fe−O−As bonds, two Fe−F−Fe bonds and one terminal -OH group. The As atom also has three As−O−Fe bonds and one terminal As−O bond. The As atom is tetrahedrally coordinated by oxygen atoms with an average As−O distance of 1.6873 Å and O−As−O bond angle of 109.4°. Using the Brown−Altermatt formalism[30] for the bond length/bond valence relationship for Fe−O and As−O, bond-order sums for the cations and anions were calculated (Table 1). The calculated bond-order sums for both cations and anions are in agreement with the formal oxidation states of +3, +5 and −2 for Fe, As and O atoms respectively.

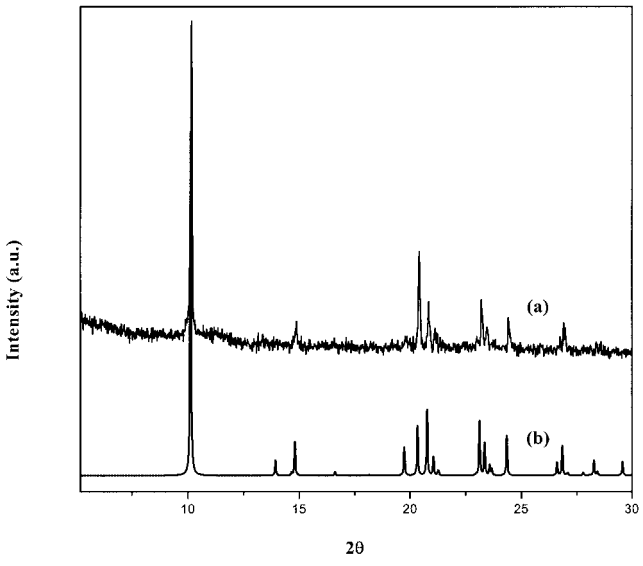

Figure 1. ORTEP diagram of $[C_{10}N_4H_{28}][\{FeF(OH)(HAsO_4)\}_4]$ showing the atoms that constitute the layer; thermal ellipsoids are given at 50% probability

The inset of Figure 2 shows the $\{FeF(OH)(HAsO_4)\}^-$ segment of the structure. As can be seen, two $FeO_3F_2(OH)$ distorted octahedra share a common edge. These dimeric units are connected by AsO_4 groups in a doubly bridging fashion. The AsO_4 units also act as a terminal ligand to the neighboring $FeO_3F_2(OH)$ octahedra. Thus, each AsO_4 unit is linked to three $FeO_3F_2(OH)$ octahedra, its fourth vertex being free and pointing into the inter-lamellar region. Similarly, each $FeO_3F_2(OH)$ octahedron links with three AsO_4 tetrahedra and connects to another Fe through the edge, with the remaining vertex, which is an -OH group, pointing into the interlayer region. The $(Fe_2F_2)^{4+}$ core and the two AsO_4 units linking it in a chelating fashion is identical to the secondary building unit SBU-4, formulated by Ferey.[28,29] Similar building units and connectivity have also been observed in A-frame compounds.[31] The SBU-4 units are linked through their corners forming an extended layered structure (Figure 2). The arrangement of layers in the *ab* plane is shown in Figure 3. As can be seen there are

Table 1. Selected bond lengths and angles for $[C_{10}N_4H_{28}][\{FeF(OH)(HAsO_4)\}_4]$ (**I**)[a]

Bond	Distance (Å)	Bond	Distance (Å)
As(1)−O(3)	1.668(6) [1.321]	Fe(1)−O(1)#1	1.928(6) [0.637]
As(1)−O(1)	1.678(6) [1.275]	Fe(1)−O(3)	1.999(6) [0.520]
As(1)−O(2)	1.689(6) 1.235]	Fe(1)−F(1)	2.011(5) [0.411]
As(1)−O(4)	1.713(6) [1.139]	Fe(1)−O(2)#2	2.028(6) [0.483]
Σ(As − O)	**[4.970]**	Fe(1)−F(1)#2	2.049(5) [0.366]
Fe(1)−O(5)	1.884(6) [0.700]	**Σ(Fe − O/F)**	**[3.117]**
Moiety	**Angle (°)**	**Moiety**	**Angle (°)**
O(3)−As(1)−O(1)	113.4(3)	O(1)#1−Fe(1)−O(2)#2	94.1(3)
O(3)−As(1)−O(2)	114.5(3)	O(3)−Fe(1)−O(2)#2	169.7(3)
O(1)−As(1)−O(2)	108.8(3)	F(1)−Fe(1)−O(2)#2	87.7(2)
O(3)−As(1)−O(4)	104.8(3)	O(5)−Fe(1)−F(1)#2	91.7(2)
O(1)−As(1)−O(4)	108.8(3)	O(1)#1−Fe(1)−F(1)#2	176.3(3)
O(2)−As(1)−O(4)	106.1(3)	O(3)−Fe(1)−F(1)#2	86.8(2)
O(5)−Fe(1)−O(1)#1	91.1(3)	F(1)−Fe(1)−F(1)#2	77.6(2)
O(5)−Fe(1)−O(3)	92.9(3)	O(2)#2−Fe(1)−F(1)#2	83.5(2)
O(1)#1−Fe(1)−O(3)	95.4(3)	As(1)−O(1)−Fe(1)#3	139.1(4)
O(5)−Fe(1)−F(1)	169.3(2)	As(1)−O(2)−Fe(1)#2	124.0(3)
O(1)#1−Fe(1)−F(1)	99.6(2)	As(1)−O(3)−Fe(1)	122.9(4)
O(3)−Fe(1)−F(1)	86.8(2)	Fe(1)−F(1)−Fe(1)#2	102.4(2)
O(5)−Fe(1)−O(2)#2	90.0(3)		

[a] Symmetry transformations used to generate equivalent atoms: #1 $-x+1, y+1/2, -z+1/2$; #2 $-x+1, -y+1, -z+1$; #3 $-x+1, y-1/2, -z+1/2$. Values in brackets are the bond valences. Their sum SVB appears in bold type at the end of the list of the distances around every cation.

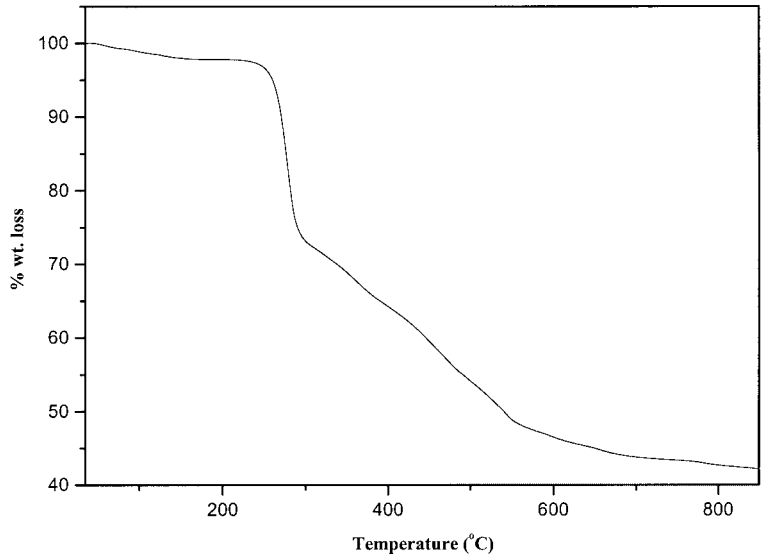

Figure 2. Polyhedral view of the structure of $[C_{10}N_4H_{28}][\{FeF(OH)(HAsO_4)\}_4]$ in the *bc* plane showing a single layer; the inset shows the SBU-4 units; the amine molecules are not shown

interactions between the layers through the terminal Fe−OH bonds.

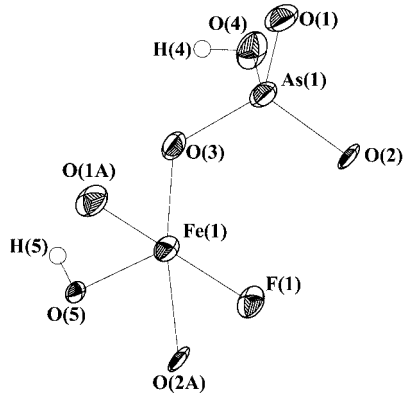

Figure 3. Polyhedral view of the structure of $[C_{10}N_4H_{28}][\{FeF(OH)(HAsO_4)\}_4]$ in the *ac* plane showing the arrangement of layers; the amine molecules are not shown for clarity; dotted lines represent possible hydrogen bond interactions

The concept of secondary building units for the description of framework structures is common in pure tetrahedral aluminosilicate and phosphate structures.[32] Recently, many secondary building units have been identified and proposed for the description of octahedral-tetrahedral frameworks.[28,29] Though many secondary building units have been identified to describe the structure of an octahedral-tetrahedral framework solid, the assembly of only one type of secondary building unit is rare. To the best of our knowledge, $[C_{10}N_4H_{28}][\{FeF(OH)(HAsO_4)\}_4]$ (**I**) is the first example possessing only the SBU-4 units, though similar layers formed by SBU-4 units are known for vanadium arsenate.[15] Similar building units of the type described here have also been observed earlier in a gallium phosphate, $[C_6N_2H_{14}][Ga_3(OH)F_3(PO_4)(HPO_4)_2]\cdot 0.5H_2O$.[33]

The variable-temperature magnetic susceptibility measurements of $[C_{10}N_4H_{28}][\{FeF(OH)(HAsO_4)\}_4]$ (**I**) were carried out on a powdered sample in the range from 4 to 300 K. Plots of the χ_m versus T is shown in Figure 4 and the inset shows the χ^{-1} versus temperature plot. The molar magnetic susceptibility increases with decreasing temperature and reaches a sharp maximum around 20 K. If T is reduced further, the susceptibility decreases very sharply. This sharp exponential decrease of magnetic susceptibility corresponds to a finite spin-gap in the system. In general, for a system with a spin-gap at low temperature, the susceptibility obeys a form given by χ (low-T) = $A\exp(-\Delta/T)/T^{\zeta}$, where A and ζ are constants and Δ represents the magnetic gap.[34,35] By fitting the experimental data at low temperature with this form of χ, we obtain a gap of about 8.1 K (with A = 2.5, and ζ = 0.6). On the other hand, the high temperature susceptibility data fits with the Curie−Weiss form χ(high-T) = C/(T-θ), with θ = −31 K and C = 16.424. High temperature χ of this form fits well with the experimental data (χ_m) up to a temperature of about 65 K.

A closer look at the magnetic lattice suggests that within the Fe_2F_2 dimers, the magnetic super-exchange is very strong, while the Fe_2F_2 dimers interact with the neighboring dimers through the AsO_4 bridges by weak super-exchange interactions. The Fe−F−Fe bond angle of 102.4° seems to favor ferromagnetic interactions, while those between the dimers through arsenate with the Fe−O−As bond angles of 128.67° favor anti-ferromagnetic interactions, according to the Goodenough rules.[36] Using the Heisenberg model for two S = 5/2 spins (dimer), the magnetic energy levels can be written as E_S = -J/2[$S(S + 1) - 35/2$] with S values 0,1,2,3,4 and 5. The magnetic susceptibility can be defined as $\chi = g^2\mu_B{}^2[\langle M^2\rangle - \langle M\rangle^2]/K_BT$, where $[\langle M\rangle^2 - \langle M\rangle^2]$ is the fluctuation in magnetization, M. For an antiferromagnet in the absence of magnetic field, the average

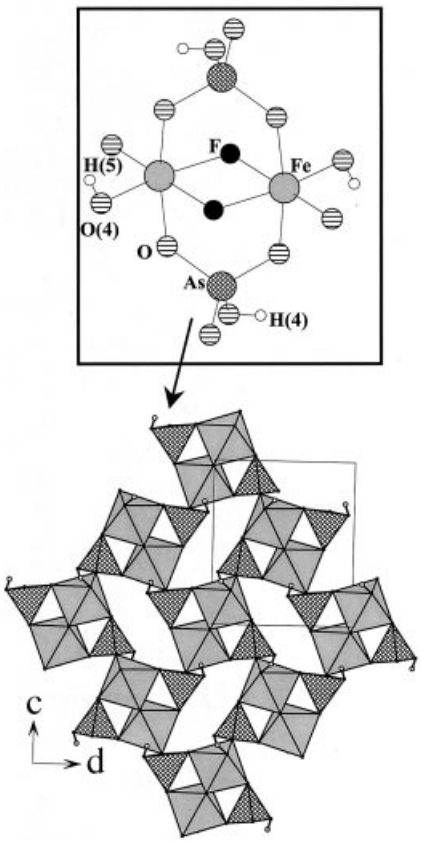

Figure 4. Thermal variation of the experimental magnetic susceptibility (χ) of $[C_{10}N_4H_{28}][\{FeF(OH)(HAsO_4)\}_4]$; the solid line is a fit using the exponential form (see text); the Inset shows the variation of inverse magnetic susceptibility (χ^{-1}) with temperature; the Curie−Weiss fit is shown as dotted lines

magnetization, <M>, vanishes. Thus the magnetic susceptibility for the dimer can be written as $\chi_{dimer} = g^2\mu_B{}^2/K_BT[\Sigma_S\{S(S+1)\exp(E_S/K_BT)\}/\Sigma_S\exp(E_S/K_BT)]$, $S = 0,1,2,3,4$ and 5. In Figure 5 we have fitted this dimer susceptibility with the experimental χ_mT, varying the exchange constant, J, and the Lande factor, g. The best fit is obtained with $g = 2.01$ and $J = -12$ K. The same $\chi_{dimer}T$ formula with fitted J and g values is used to calculate the effective magnetic moment. The effective magnetic moment (μ_{eff}) appears to compare well with the presence of iron in the +3 state. Note that the dimer model cannot adequately reproduce the experimental data over all the temperatures. The lowest magnetic gap is 12 K (−J) from the dimer model, while the fit of the low temperature χ_m gives a gap of about 8.1 K (Δ). This discrepancy can be attributed to the neglect of inter-dimer exchange interactions in the dimer model. More work is clearly necessary to understand the significance of inter-dimer exchange interactions in two-dimensional systems.

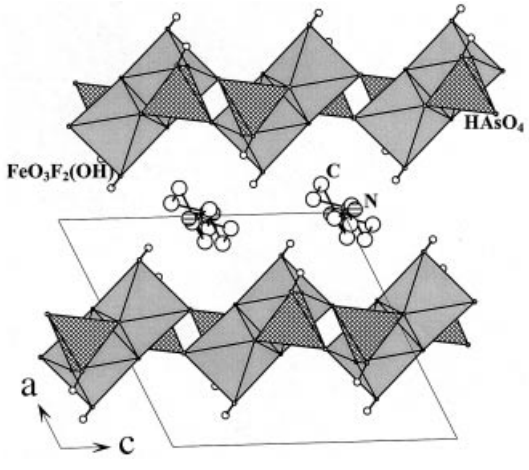

Figure 5. The variation of the χT as a function of temperature for $[C_{10}N_4H_{28}][\{FeF(OH)(HAsO_4)\}_4]$; the inset shows the variation of $\mu_{eff.}$ as a function of temperature; the solid line in both the cases shows the dimer-model fit to the experimental data

Conclusions

In conclusion, a new layered Fe^{III} arsenate, $[C_{10}N_4H_{28}][\{FeF(OH)(HAsO_4)\}_4]$, has been prepared in the presence of 1,4-bis(3-aminopropyl)piperazine by employing hydrothermal methods. The formation of the layered structure based purely on only one type of building unit (SBU-4) and its assembly through their corners are noteworthy structural features. Our continuing investigations clearly reveal that the chemistry of inorganic compounds possessing octahedral-tetrahedral building units is rich and many more novel structures are likely to be discovered. We are currently pursuing this theme.

Experimental Section

Synthesis and Initial Characterization

Solvothermal reactions were carried out under autogenous pressure in PTFE-lined stainless steel acid digestion bombs. For the preparation of $[C_{10}N_4H_{28}][\{FeF(OH)(HAsO_4)\}_4]$ (**I**) a mixture of iron chloride hexahydrate $[FeCl_3{\cdot}6H_2O]$ (0.1487 g), arsonic acid (0.6248 g), AP-PIP (0.441 g), HF (48%, 0.12 mL), water (4 mL) and *n*-hexanol (2 mL) were taken in the ratio 1:8:4:6:400:29. The mixture was homogenized at room temperature for 30 min and heated

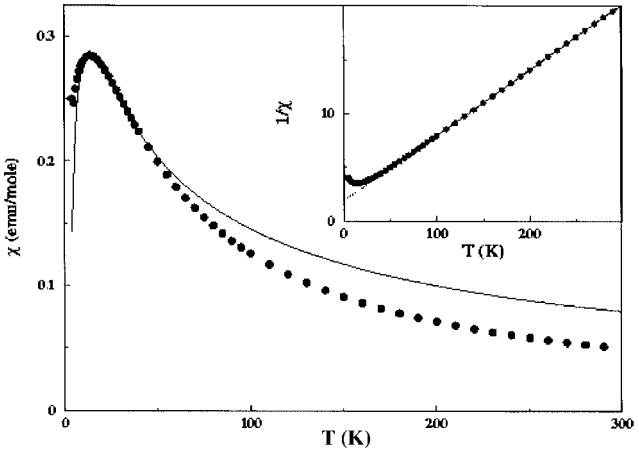

Figure 6. Powder XRD pattern of $[C_{10}N_4H_{28}]$-$[\{FeF(OH)(HAsO_4)\}_4]$ (a) experimental (Cu $K\alpha$) and (b) simulated

at 150 °C for 72 h. The initial pH of the reaction mixture was about 2 and there was no appreciable change in the pH after the reaction. The resulting product, a crop of colorless plate-like crystals, was filtered, washed with water, and dried at room temperature [yield = 70% based on Fe]. A microanalysis of this phase by energy-dispersive X-ray fluorescence indicated the presence of As and Fe in a 1:1 ratio. $[C_{10}N_4H_{28}][\{FeF(OH)(HAsO_4)\}_4]$ (1131.07): calcd. C 10.6, H 3.18, N 4.95; found C 10.1, H 3.01, N 4.89. A chemical analysis also confirmed the presence of fluorine (calcd. 6.65%; found 6.5%).[37]

The product contained a single crystalline phase as judged by a comparison of the powder pattern with the pattern simulated from the atomic coordinates obtained from the single crystal structure analysis (Figure 6). A least-squares fit of the powder XRD (Cu *Kα* radiation) lines, using the *hkl* indices garnered from single-crystal data, gave the following cell: a = 9.5941(3), b = 8.3335(4), c = 10.7420(4) Å, β = 114.99(3)°. The cell parameters are in good agreement with those determined from the single crystal XRD.
Thermogravimetric analysis (TGA) of $[C_{10}N_4H_{28}][\{FeF(OH)(HAsO_4)\}_4]$ (**I**) was carried out under N_2 (flow rate = 50 mL/min) in the range between 25 and 700 °C (heating rate = 10 °C/min) (Figure 7). A small initial weight loss of about 2% observed in the region 25−200 °C, probably corresponds to the loss of some adsorbed water on the surface of the sample. Similar initial weight losses have been encountered in many solids with open-framework structures. The TGA shows a sharp weight loss in the region 250−300 °C followed by a tail up to 600 °C. The total weight loss of 57% corresponds very well with the loss of the amine, fluoride, the condensation of the -OH groups and the partial removal of As_2O_5 (calcd. 57.5%). The powder XRD showed the resulting decomposed powder to be amorphous.

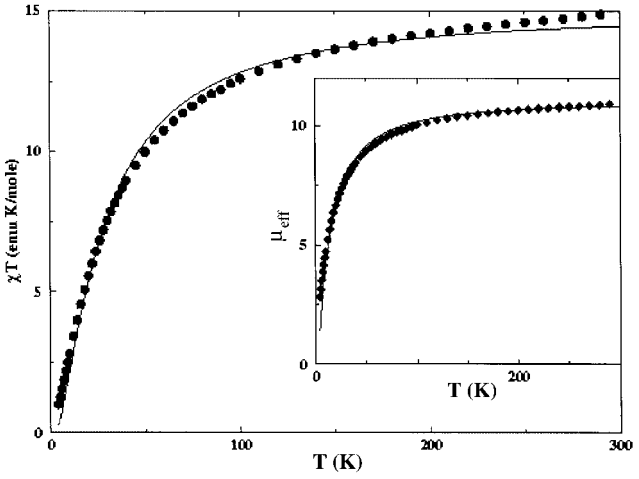

Figure 7. Thermogravimetric analysis (TGA) of $[C_{10}N_4H_{28}][\{FeF(OH)(HAsO_4)\}_4]$

Infrared (IR) spectra of $[C_{10}N_4H_{28}][\{FeF(OH)(HAsO_4)\}_4]$ (**I**) was recorded in the range 400−4000 cm^{-1} using the KBr pellet method. The IR spectra showed typical peaks with absorption bands for N−H, C−H and O−H bending and stretching vibrations: ν_s(OH) = 3426 cm^{-1} (vb), ν_s(NH) = 2873 (w), $\delta_s(NH_2)$ = 1619 cm^{-1} (s) and 1524 (s) cm^{-1}, $\delta(N^+\text{-}CH_2$ asym. drift) = 1480 cm^{-1} (m), ν_s(C−N) = 843 cm^{-1} (s), $\rho_r(CH_2)$ = 767 cm^{-1} (m), $\nu(NH_2^+)$ = 2373 cm^{-1} (m) and ν(C−C) = 1058 cm^{-1} (w).

Single-Crystal Structure Determination

A suitable colorless single crystal was carefully selected under a polarizing microscope and glued to a thin glass fiber with cyanoacrylate (superglue) adhesive. Crystal structure determination by X-ray diffraction was performed on a Siemens SMART-CCD diffractometer equipped with a normal focus, 2.4 kW sealed tube X-ray source (Mo-K_α radiation, λ = 0.71073Å) operating at 40 kV and 40 mA. A hemisphere of intensity data was collected at room temperature in 1321 frames with ω scans (width of 0.30° and exposure time of 20 s per frame) in the 2θ range 3 to 46.5°. Pertinent experimental details for the structure determination of $[C_{10}N_4H_{28}][\{FeF(OH)(HAsO_4)\}_4]$ (**I**) are presented in Table 2.

Table 2. Crystal data and structure refinement parameters for $[C_{10}N_4H_{28}][\{FeF(OH)(HAsO_4)\}_4]$ (**I**)

Empirical formula	$C_{10}N_4H_{36}Fe_4F_4As_4O_{20}$
Formula mass	1131.07
T (K)	293(2)
Space group	$P2_1/c$ (No. 14)
a (Å)	9.6320(3)
b (Å)	8.3598(3)
c (Å)	10.7794(1)
β (°)	115.036(1)
V (Å^3)	786.42(4)
Z	4
D_{calcd} (g cm^{-3})	2.378
μ (mm^{-1})	6.093
R indexes [$I > 2\sigma(I)$]	R_1 = 0.0497;[a] wR_2 = 0.1238[b]
R (all data)	R_1 = 0.0729; wR_2 = 0.1366

[a] $R_1 = \Sigma||F_0| - |F_c||/\Sigma|F_0|$. [b] $wR_2 = \{\Sigma[w(F_0^2 - F_c^2)^2]/\Sigma[w(F_0^2)^2]\}^{1/2}$. $w = 1/[\sigma^2(F_0)^2 + (aP)^2 + bP]$, $P = [\max.(F_0^2,0) + 2(F_c)^2]/3$, where a = 0.0738 and b = 0.0.

An absorption correction based on symmetry equivalent reflections was applied using the SADABS program (maximum and minimum effective transmission: 1.000000, 0.639708).[38] Other effects, such as absorption by the glass fiber, were simultaneously corrected. The structures were solved by direct methods and in each case, a sufficient fragment of the structure was revealed (As, Fe and O) to enable the remainder of the non-hydrogen atoms to be located from difference Fourier maps and the refinements to proceed to $R <$ 10%. Fluorine atoms, identified by chemical analysis, were localized after consideration of thermal motion parameters and bond valence calculations.[30] The amine molecule was disordered and a model was established based on the observed positions of the various peaks in the difference Fourier map, resulting in shorter C−C distances and angles. Geometric constraints on the bond lengths have been used to keep the molecule in position during the refinement cycles. The disorder of the amine molecule also precluded the anisotropic refinement of the C and N atoms. No hydrogen atoms corresponding to the amine molecules were found in the difference Fourier map and hence were not included. The hydrogen atoms attached to the oxygen atoms [O(4) and O(5)] were placed and held in the riding mode during the refinement cycles. The last cycles of refinement included atomic positions for all the atoms, anisotropic thermal parameters for all non-hydrogen framework atoms, isotropic thermal parameters for all the hydrogen atoms attached to the oxygen atoms. Full-matrix least-squares refinement against $|F^2|$ was carried out using the SHELXTL-PLUS[39] suite of programs. Details of the final refinement are given in Table 2. The selected bond lengths and angles are given in Table 1. CCDC-204836 contains the supplementary crystallographic data for this paper. These data can be obtained free of charge at www.ccdc.cam.ac.uk/conts/

retrieving.html [or from the Cambridge Crystallographic Data Centre, 12, Union Road, Cambridge CB2 1EZ, UK; Fax: (internat.) +44-1223/336-033; E-mail: deposit@ccdc.cam.ac.uk].

Acknowledgments

The authors thank Prof. C.N.R. Rao, FRS for his support. SN thanks the Department of Science and Technology (DST), Government of India for the award of a research grant.

[1] A. K. Cheetham, T. Loiseau, G. Ferey, *Angew. Chem. Int. Ed.* **1999**, *38*, 3268 and references cited therein.
[2] M. Riou-Cavellec, D. Riou, G. Ferey, *Inorg. Chim. Acta* **1999**, *291*, 317 and references cited therein.
[3] K.-H. Lii, Y.-F. Huang, V. Zima, C.-Y. Huang, H.-M. Lin, Y.-C. Jiang, F.-L. Liao, S.-L. Wang, *Chem. Mater.* **1998**, *10*, 2599 and references cited therein.
[4] A. Choudhury, S. Natarajan, C. N. R. Rao, *Chem. Commun.* **1999**, 1305.
[5] R. D. Shannon, *Acta Crystallogr., Sect. A* **1976**, *32*, 751.
[6] W. T. A. Harrison, M. L. F. Phillips, A. V. Chavez, T. M. Nenoff, *J. Mater. Chem.* **1999**, *9*, 3087.
[7] P. Feng, T. Zhang, X. Bu, *J. Am. Chem. Soc.* **2001**, *123*, 8608.
[8] J. Chen, R. Xu,, *J. Solid State Chem.* **1989**, *80*, 149.
[9] J. Chen, L. Li, G. Yang, R. Xu, *J. Chem. Soc., Chem. Commun.* **1989**, 1217.
[10] X. Bu, P. Feng, T. E. Gier, G. D. Stucky, *J. Solid State Chem.* **1998**, *136*, 210.
[11] R. C. Haushalter, Z. Wang, L. M. Meyer, S. S. Dhingra, M. E. Thompson, J. Zubieta, *Chem. Mater.* **1994**, *6*, 1463.
[12] K.-F. Hsu, S.-L. Wang, *Chem. Mater.* **1999**, *11*, 1876.
[13] M.-Y. Lee, S.-L. Wang, *Chem. Mater.* **1999**, *11*, 3588.
[14] C. A. Bremner, W. T. A. Harrison, *Acta Crystallogr.* **2002**, *E58*, m319.
[15] F. Gagnard, C. Reisner, W. Tremel, *Inorg. Chem.* **1997**, *36*, 352.
[16] L.-H. Huang, H.-M. Kao, K.-H. Lii, *Inorg. Chem.* **2002**, *41*, 2936.
[17] S.-L. Wang, Y.-H. Lee, *Inorg. Chem.* **1994**, *33*, 3845.
[18] A.-H. Liu, S.-L. Wang, *Inorg. Chem.* **1998**, *37*, 3415.
[19] Y.-C. Liao, S.-H. Luo, S.-L. Wang, H.-M. Kao, K.-H. Lii, *J. Solid State Chem.* **2000**, *155*, 37.
[20] S.-H. Luo, Y.-C. Jiang, S.-L. Wang, H.-M. Kao, K.-H. Lii, *Inorg. Chem.* **2001**, *40*, 5381.
[21] B. Bazan, J. L. Mesa, J. L. Pizarro, L. Lezama, M. I. Arriortua, T. Rojo, *Inorg. Chem.* **2000**, *39*, 6056.
[22] S. Ekambaram, S. C Sevov, *Inorg. Chem.* **2000**, *39*, 2405.
[23] S. Chakrabarti, S. Natarajan, *Angew. Chem. Int. Ed.* **2002**, *41*, 1224.
[24] B. Bazan, J. L. Mesa, J. L. Pizarro, A. Goni, L. Lezama, M. I. Arriortua, T. Rojo, *Inorg. Chem.* **2001**, *40*, 5691.
[25] N.-Y. Fan, S.-L. Wang, *Inorg. Chem.* **1996**, *35*, 4708.
[26] S. Chakrabarti, S. Natarajan, *J. Chem. Soc., Dalton Trans.* **2002**, 3874.
[27] S. Chakrabarti, S. Natarajan, *J. Chem. Soc., Dalton Trans.* **2002**, 4156.
[28] G. Ferey, *J. Fluorine Chem.* **1995**, *72*, 187 and the references therein.
[29] G. Ferey, *Chem. Mater.* **2001**, *13*, 3084 and the references therein.
[30] I. D. Brown, D. Altermatt, *Acta Crystallogr., Sect. B* **1985**, *41*, 244.
[31] D. M. Hoffman, R. M. Fisel, R. H. Hoffman, *J. Am. Chem. Soc.* **1982**, *104*, 3859.
[32] *Atlas of Zeolite Framework Types* (Eds. Ch. Baerlocher, W. H. Meier and D. H. Olson), Elsevier, NY, 2001.
[33] T. Loiseau, G. Ferey, *J. Chem. Soc., Chem. Commun.* **1992**, 1197.
[34] J. W. Bray, L. V. Interrante, I. S. Jacobs and J. C. Bonnere, *Extended Linear Chain Compounds* (Ed. J. S. Miller), Plenum, New York, 1985, p.353.
[35] M. Troyer, H. Tsunetsugu, D. Wurtz, *Phys. Rev. B* **1994**, *50*, 13515.
[36] J. B. Goodenough, *Magnetism and the Chemical Bond*; Interscience; New York, 1963.
[37] *Vogel's Textbook of Quantitative Chemical Analysis*, Vth Edition, John Wiley & Sons Inc., New York, (1989).
[38] G. M. Sheldrick, *SADABS Siemens area detector absorption correction program*, University of Gottingen, Germany (1994).
[39] G. M. Sheldrick, *SHELX-97 A program for crystal structure solution and refinement*, University of Gottingen, Germany (1997).

Received April 25, 2003

